Cloud-to-Ground Lightning Observations from TOGA COARE: Selected Results and Lightning Location Algorithms

WALTER A. PETERSEN AND STEVEN A. RUTLEDGE

Department of Atmospheric Science, Colorado State University, Fort Collins, Colorado

RICHARD E. ORVILLE

Cooperative Institute for Applied Meteorological Studies, Department of Meteorology, Texas A&M University, College Station, Texas

(Manuscript received 15 February 1995, in final form 16 October 1995)

ABSTRACT

Recently, observations of electrified oceanic convection and associated cloud-to-ground (CG) lightning were obtained over the tropical western Pacific Ocean during TOGA COARE (Tropical Ocean Global Atmosphere Coupled Ocean–Atmosphere Response Experiment). During COARE, observations of convection were made using a variety of instrument platforms including ship and airborne Doppler radars, an advanced lightning direction finder (ALDF) network, and a shipborne inverted electric field mill. This study focuses on data collected by the COARE ALDF network, fusion of those data with observations, and the methods used to calculate accurate CG return stroke locations.

Analysis of CG lightning data and Doppler radar data indicates that lightning-producing oceanic convection is characterized by deep, vertically developed convective cells with radar reflectivities exceeding 30 dBZ above the height of the −10°C level. In several cases a peak in CG frequency occurred coincident with the descent of precipitation mass bounded by the 30-dBZ reflectivity contour, linking the descent of the hydrometeor mass to the occurrence of CG lightning. The diurnal cycle of oceanic CG lightning, the convective available potential energy (CAPE), and rainfall indicates a peak in all these variables in the early morning hours (local time), approximately 2 h before the peak in cold-cloud area defined by brightness temperatures of less than −65°C. Sounding data indicate a strong positive correlation between CAPE and mixed-layer wet-bulb potential temperature and a weak positive correlation between CAPE and the number of CG lightning flashes observed in a 24-h period. The data also indicate that a highly nonlinear relationship exists between the wet-bulb potential temperature and the number of CG flashes observed in a 24-h period.

1. Introduction

Satellite observations of lightning over the oceans (e.g., Orville and Spencer 1979; Turman and Edgar 1982; Orville and Henderson 1986) have provided statistics such as lightning flash densities over the oceans or ratios of the total number [*in-cloud and cloud-to-ground* (CG)] of continental to oceanic lightning flashes. However, this method of observation does not permit the coincident examination of storm electrification processes relative to the convective life cycle (i.e., the dynamical and microphysical evolution of the electrified oceanic convection). Studies that have examined the convective *and* electrical life cycles of oceanic storms are relatively few in number and have been limited primarily to observations taken along coastlines (e.g., Chauzy et al. 1985; Rutledge et al. 1992; Williams et al. 1992; Petersen and Rutledge 1992; Kitagawa and Michimoto 1994; Rutledge and Petersen 1994) or islands (e.g., Takahashi 1978, 1983; Hojo et al. 1989; Takahashi and Kuhara 1993). Observations of CG lightning over remote regions of the earth's oceans are even more limited. Coincident observations of the electrical (including CG and in-cloud lightning), microphysical, and dynamical evolution of maritime thunderstorms in remote oceanic environments has proven to be a difficult task from both practical and logistical standpoints.

Recently, however, observations of electrified oceanic convection and associated cloud-to-ground lightning were obtained over remote regions (Fig. 1) of the tropical western Pacific Ocean (equatorial warm-pool) during the Tropical Ocean Global Atmosphere Coupled Ocean–Atmosphere Response Experiment (TOGA COARE) (Webster and Lukas 1992). These observations were obtained using several different instrument platforms including a three-station advanced lightning detection and location network [advanced lightning di-

Corresponding author address: Dr. Steven A. Rutledge, Department of Atmospheric Science, Colorado State University, Fort Collins, CO 80523.
E-mail: rutledge@olympic.atmos.colostate.edu

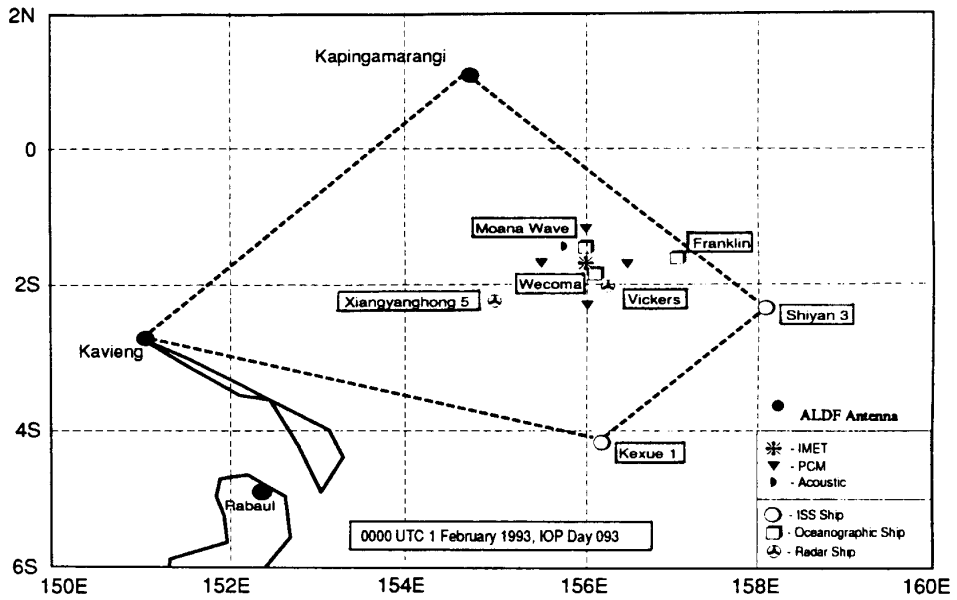

FIG. 1. Map of the COARE intensive flux array (enclosed by dashed line) with the position of ships and moorings at 0000 UTC 1 February 1993. Dark filled circles indicate the positions of ALDF antennas at Kapingamarangi Atoll, Kavieng, and Rabaul (adapted from the TOGA COARE Intensive Operations Summary).

rection finder (ALDF) network; Orville et al. 1994], a variable gain flat plate antenna (operated by M. Brook, New Mexico Institute of Mining and Technology, and described in Orville et al. 1994), shipboard and airborne Doppler radars (Rutledge et al. 1993; Jorgensen et al. 1996), and shipboard and airborne electric field mills (Petersen et al. 1993; Blakeslee and Christian 1994). Additionally, a large number of other instrument platforms were deployed during TOGA COARE (e.g., the sounding network; Johnson et al. 1993) that are useful for examining the ambient conditions and forcing associated with electrified oceanic clouds.

In this study we first focus on data collected by the COARE ALDF network and the application of those data to studies of electrified convection on the cloud scale. We follow those analyses with an examination of the relationship between CG lightning and the large scale, comparing CG flash frequencies to variables such as the convective available potential energy (CAPE) mixed-layer wet-bulb potential temperature, rainfall, and cold-cloud area coverage over the western Pacific warm pool. Before specific cases of electrified convection are examined, we briefly describe the TOGA COARE ALDF network and the algorithms used to locate cloud-to-ground lightning flashes that occurred in the vicinity of the TOGA COARE intensive flux array (IFA; Fig. 1). The details of algorithms used to locate the flash positions are provided in the appendix.

2. The TOGA COARE ALDF network

During the months November–December 1992, three high-gain ALDF antennas manufactured by LLP (Lightning Location and Protection Inc., Tucson, Arizona) were installed at Kavieng, Papua New Guinea (PNG), Rabaul PNG, and Kapingamarangi Atoll (2.58°S, 150.81°E; 4.22°S, 152.18°E; and 1.07°N, 154.81°E, respectively; Fig. 1). The three-station network became fully operational in late December 1992, and data continued to be collected through virtually all of 1993. The data collected by the ALDF network for each CG stroke included the time of occurrence [to the nearest microsecond and time stamped at each antenna using a global positioning satellite (GPS) receiver], azimuth, polarity, and the electric and magnetic field strengths.

Because the COARE ALDF network needed to accurately detect and locate CG return strokes that occurred within the IFA (Fig. 1), the required maximum effective range of the network was on the order of 900 km. This range far exceeds the 600-km maximum previously recommended for use in ALDF networks (Brook et al. 1989). Therefore, to extend the effective range of the network, the antenna gains were increased by a factor of 1.5 (Orville et al. 1994) and the waveform acceptance criteria were adjusted to increase the sensitivity of the network (e.g., the pulse width acceptance was decreased, and the bipolar reject and ''second peak greater than'' ratios were increased). However, the increased sensitivity of the ALDFs also increased the probability of detecting nearby intracloud flashes. To examine this problem, independent waveform analyses using flat plate antenna data are currently being undertaken by M. Brook at the New Mexico Institute of Mining and Technology. Using flash data col-

lected simultaneously by the ALDF network and the flat plate antenna, it may be possible to determine both the percentage of intracloud flashes detected by the lightning network and the network detection efficiency. For studies of electrified convection at moderate distances from the ALDF network (e.g., near the shipboard radars), the occurrence of anomalous CG locations due to in-cloud lightning detection by the network is not expected to be a problem.

In contrast to lightning location networks operated in the United States and other areas of the world, no central position analyzer (e.g., Orville et al. 1983) was used to locate the CG lightning in real time because of the remote nature of the ALDF sites. Thus, the data were collected and stored at each ALDF site and analyzed after the data were later returned to the United States. Due to the limited number of sites at which the antennas could be installed, there were towers, fences, and buildings located near the direction finders. Therefore, site errors in the measured azimuth bearings were potentially quite large. Fortunately, each ALDF antenna in the network was connected to an absolute time source (GPS clock) that enabled time-of-arrival methods (e.g., Hughes and Gallenberger 1974) to be used to accurately determine *flash* locations and site errors at each antenna location (herein, *flash* refers to a set of cloud-to-ground return *strokes* separated by less than 500 ms in time of occurrence and less than 10 km in distance; e.g., Uman 1987; Watson and Holle 1994).

Typically, lightning location networks using magnetic direction finder antennas, such as the National Lightning Detection Network (NLDN) in the United States, rely on magnetic direction-finding algorithms (e.g., Krider et al. 1976) for locating cloud-to-ground flashes. Magnetic direction finding uses simple triangulation based on the intersection of azimuth bearings from two or more cross-looped antennas to locate a flash. Other networks such as the Lightning Processing and Tracking System (LPATS; Bent and Lyons 1984) rely solely on the use of time-of-arrival (TOA) location methods to find the position of a lightning flash. For TOA-type systems, a flash is located by calculating the intersection of two or more hyperbolas whose equations are determined by the difference in flash electromagnetic wave arrival times at three or more antennas. In the past, both TOA and magnetic direction-finding techniques have been used in a mutually exclusive fashion. To locate CG return strokes (which were later combined to form flashes) over the moderate-to-long ranges associated with the COARE domain, we developed magnetic direction-finding algorithms, TOA algorithms, and a ''hybrid'' TOA algorithm that used the triangulated return stroke position as an initial guess in the process of calculating a TOA-type solution from the intersection of two hyperbolas.

The TOA and hybrid TOA location techniques produced the most accurate CG locations (estimated to be within about 10 km of the true location over distances approaching 900 km from the network) and were found to be more suitable for use in spatially detailed analyses, for example, assigning a particular CG flash to a particular convective feature as identified by radar. Flash locations calculated with magnetic direction-finding appeared to be less accurate (i.e., errors often exceeded 10 km at distances of 300 km from the center of the network) but were still of great use in larger-scale applications (e.g., flash density calculations over large areas, etc.). A more detailed description of the magnetic direction-finding, TOA, and hybrid TOA lightning location techniques is provided in the appendix.

3. Selected observations

In this section we present cloud-to-ground lightning, radar reflectivity, electric field mill, and geosynchronous meteorological satellite (GMS) satellite data for cases that occurred on 1, 9, and 15 February 1993. The data presented for 1 February 1993 are radar, electric field, and cloud-to-ground lightning *return stroke* data (note for this case that return strokes instead of flashes are used to enable comparison with Fig. A1 in the appendix). For the 15 February case, the radar and cloud-to-ground lightning *flash* data for four separate convective systems (no electric field data) have been composited. To more meaningfully compare the composited observations from 15 February 1993 to previous studies of electrified convection, we compiled CG *return strokes* into CG *flashes* according to the definition given in section 2. The composite is presented in the form of a time–height–reflectivity diagram with the average number of CG flashes that occurred in 20-min time intervals also indicated. The data from 15 February 1993 are composited to clearly illustrate, *via a single diagram*, the vertical and electrical evolution of the storms that occurred on this day. We conclude this section with geosynchronous meteorological satellite (GMS) observations of electrified convection (cloud-to-ground lightning return stroke locations overlaid) from 9 February 1993.

a. Lightning-producing convection that occurred on 1 February 1993

On 1 February 1993, deep, widespread convection occurred within range of the Massachusetts Institute of Technology (MIT) radar on board the R/V *John V. Vickers* and was organized into eastward moving short lines with random orientations. Cloud-to-ground lightning activity occurred in isolated clusters throughout the COARE domain. An example of the electrified convection and CG lightning that occurred this day is shown in Fig. 2. Figure 2 indicates that cloud-to-ground return strokes were located in the vicinity of reflectivity maxima situated approximately 13 and 64 km northeast of the MIT radar. A time series of vertical cross sec-

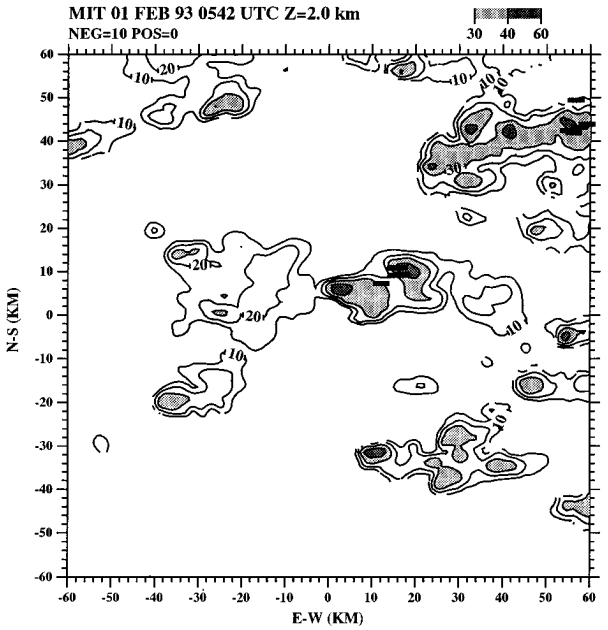

FIG. 2. Horizontal cross section of radar reflectivity centered on the MIT radar (0, 0) at an elevation of 2 km for 0542 UTC 1 February 1993. The contour interval is 10 dBZ. Reflectivities greater than 30 dBZ are lightly shaded, with heavier shading indicating values in excess of 40 dBZ. Negative cloud-to-ground return stroke positions (calculated with the hybrid TOA algorithm) for a 20-min interval centered on the time of the CAPPI are indicated by a dash.

tions through the deepest parts of the two sets of lightning-producing cells is shown in Fig. 3.

Note the change in height of the 30-dBZ reflectivity contour with time in the cross sections. We use this contour as a proxy for the boundary of the convective reflectivity ''core.'' Similar to previous observations of electrified convection over regions of the maritime continent (Williams et al. 1992; Rutledge et al. 1992; Zipser and Lutz 1994) and the western Pacific warm pool (Petersen et al. 1993), the reflectivity cores extended well into the region of the clouds where mixed phase conditions are possible (0° to −40°C), coincident with the time at which large surface electric fields and lightning were noted. This is an indication that updraft speeds and hydrometeor masses were large enough to allow significant charge generation to occur in the cloud (e.g., Williams and Lhermitte 1983). It is also interesting to note that the peak in CG activity and the maximum reflectivity core depth (as sampled by the radar every 10 min) appeared to be slightly out of phase in both sets of convective cells (Figs. 3a–f), with cores reaching peak heights as much as 0–10 min before to the peak in CG activity (after 0532 UTC for both sets of cells). The trend of increasing CG flash rate with the peak and subsequent descent of the reflectivity core in the mixed phase region of the cloud has been observed in several other cases from COARE and is also consistent with the findings of many previous studies conducted in other regions of the globe (e.g., Workman and Reynolds 1949; Lhermitte and Williams 1984; Williams et al. 1989; Carey and Rutledge 1996).

Figure 4 shows the electric field data (low-gain channel; 0428–0548 UTC) associated with several cells that were located in the immediate vicinity of the radar. The peak in the vertical component of the dc electric field (10–15 kV m^{-1}) occurred near 0447 UTC as a rapidly electrifying cell that moved directly over the ship. Note also the rapid excursion to a fair weather electric field that occurred at 0450 and 0455 UTC. These field excursions were likely associated with precipitation (e.g., Krehbiel 1986) because rainfall rates exceeded 70 mm h^{-1} at the ship near these times. There were some indications of lightning in the electric field trace from 0445 to 0450 UTC, though no thunder was reported at the ship. The first cloud-to-ground lightning flash (confirmed visually) occurred near 0515 UTC and was associated with one of the cells shown in Fig. 2 (cell located 13 km northeast of the radar). This CG flash occurred nearly coincident with the time the first well-defined, sharp electric field perturbation due to lightning was detected by the field mill (~0516 UTC). Because the field mill sensitivity decreased rapidly with range, it is likely that the higher-amplitude perturbations detected by the field mill were associated with CGs that occurred near the ship (i.e., within a range of 20 km). After comparing the time and number of flashes detected by the field mill with those detected coincidentally by the ALDF network, it is apparent *for this case* that the network detected all of the CG flashes that occurred near the ship (this assumes that the higher-amplitude perturbations registered by the low-gain channel of the field mill were in fact CGs and not in-cloud flashes). Between 0519 and 0534 UTC (when no CGs were detected by the network) the field mill detected many smaller-amplitude perturbations in the electric field, which were probably in-cloud (IC) flashes.

The coevolving electric field signatures, lightning, and reflectivity fields associated with the cells observed near the R/V *Vickers* on 1 February 1993 suggest that IC flashes occurred before the majority of the CG flashes (with the exception of the CG at 0516 UTC), during intensification of the cells aloft. Only after the cells reached the mature stage (peak echo-top heights, descent of the echo core), did both the field mill and the COARE ALDF network indicate a switch to predominantly CG lightning. The observed tendency for the peak in CG lightning to follow that of the IC lightning is similar to observations previously collected in the midlatitudes by Williams et al. (1989).

One important thing to note with regard to the electrified oceanic cells observed during COARE is that the oceanic cells often produced heavy rainfall at the surface well before the occurrence of any lightning

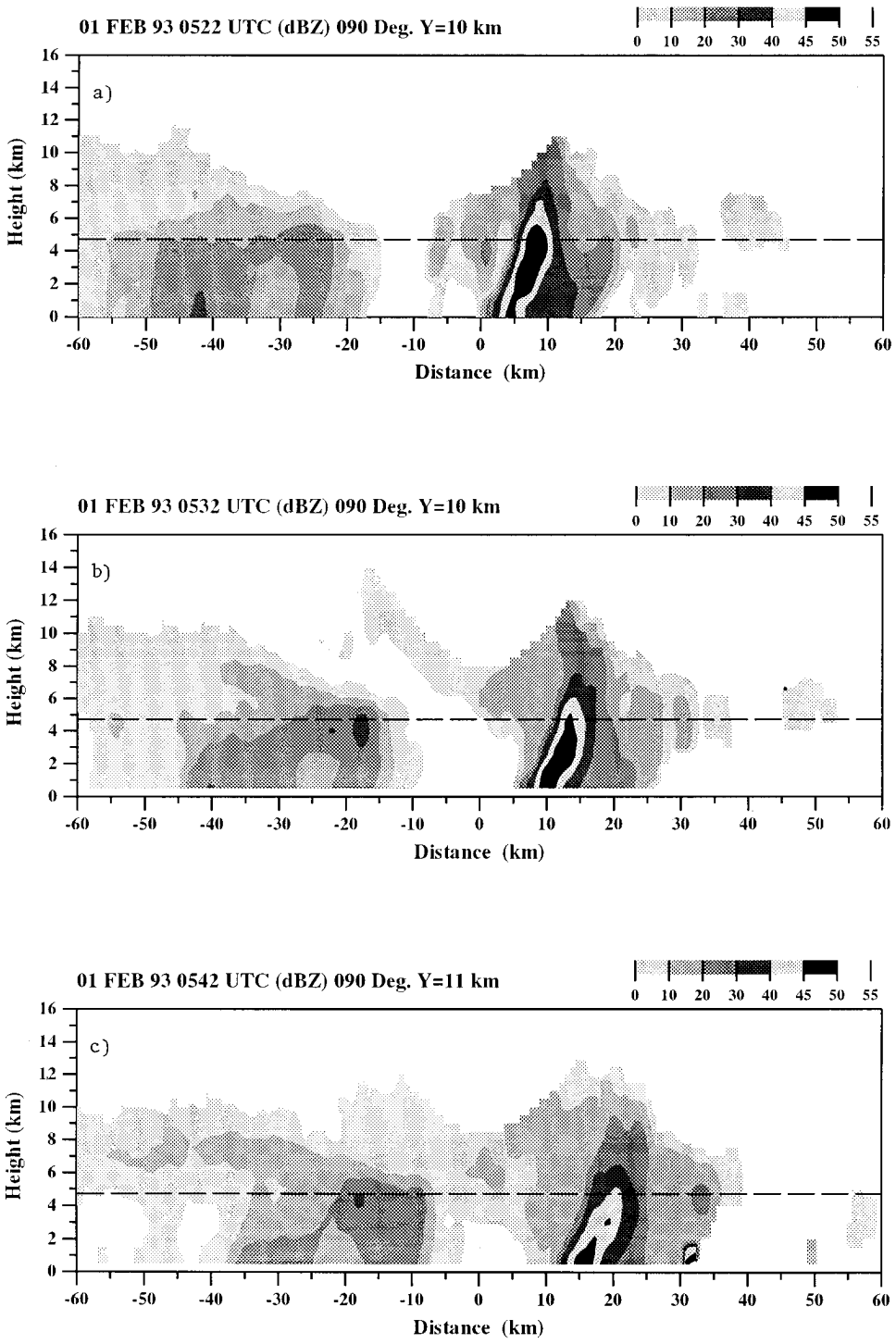

FIG. 3. Vertical cross sections of MIT reflectivity parallel to the *x* axis in Fig. 2. (a) $y = 10$ km, 0522 UTC; (b) $Y = 10$ km, 0532 UTC; (c) $Y = 11$ km, 0542 UTC; (d) $Y = 43$ km, 0522 UTC; (e) $Y = 43$ km, 0532 UTC; (f) $Y = 44$ km, 0542 UTC. The dashed line is located at the approximate height of the 0°C level.

(similar to observations by Chauzy et al. 1985). This was due to the likely presence of efficient warm rain coalescence in the COARE convective cells, a phenomenon often associated with maritime convective rainfall (see Young 1993). The occurrence of lightning (both IC and CG) in the majority of the cases

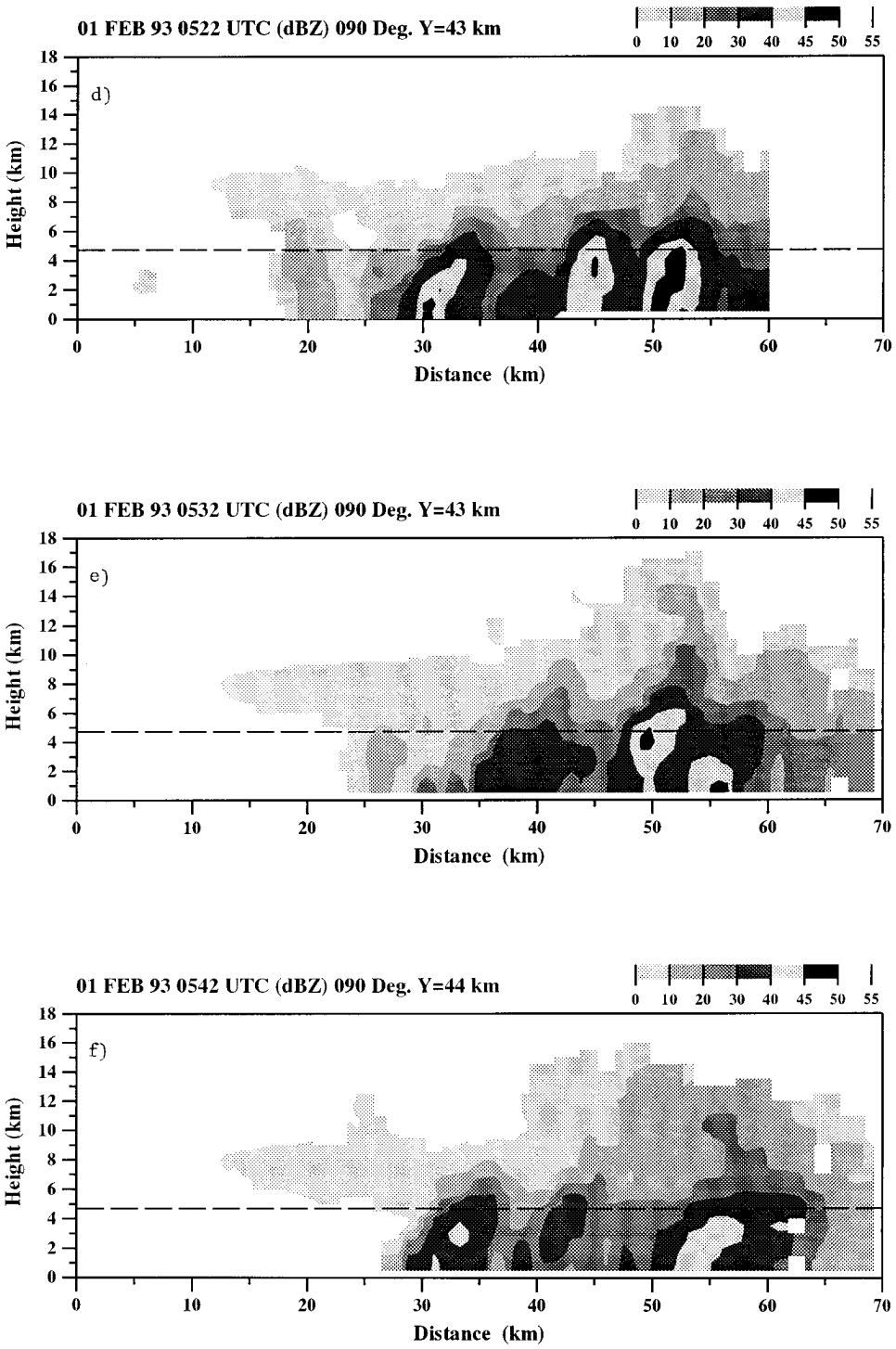

FIG. 3. (*Continued*)

examined from COARE (e.g., 1 February 1993), took place only *after* significant hydrometeor mass developed in the mixed phase region of the cloud above the −10°C level. This strongly links the occurrence of lightning in these cells to the development of moderate concentrations of precipitation-sized ice particles aloft, but not necessarily to the presence or intensity of rainfall at the surface.

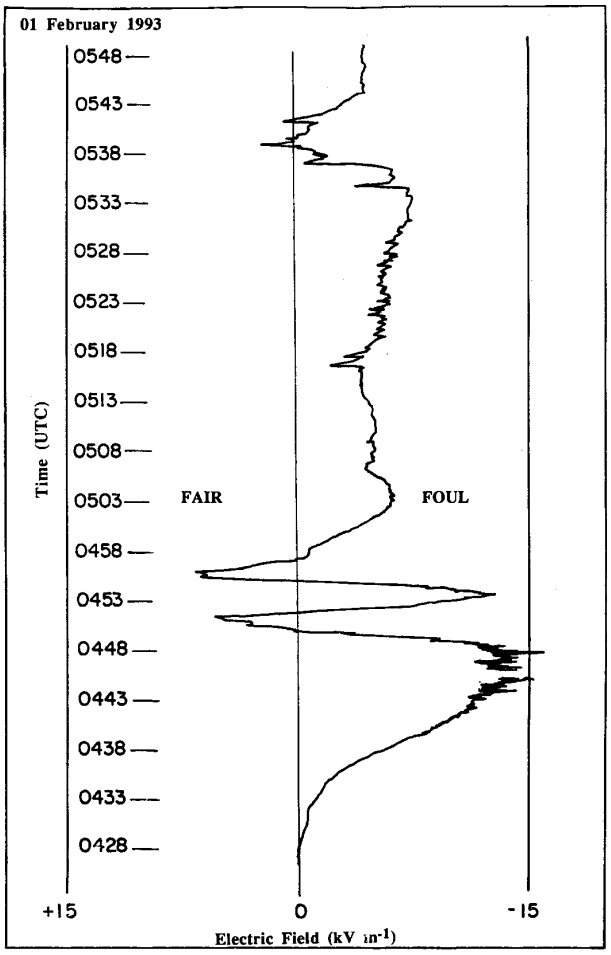

FIG. 4. Electric field data (low-gain trace) for 0428–0548 UTC 1 February 1993. The magnitude of the electric field (kV m^{-1}) is plotted on the horizontal axis, and time (UTC) is plotted on the vertical axis.

b. 15 February 1993

On 15 February, four lightning-producing convective cells occurred within 100 km of the MIT radar. The radar reflectivity structure and observed cloud-to-ground lightning patterns were very similar between each of these cells. Furthermore, each cell exhibited a life cycle of approximately 60 min. Because of the similarities in radar structure, lightning evolution, and life cycle, we chose to composite these observations into one ''representative electrified cell'' (REC). The resulting composite (Fig. 5) represents the growth and decay with time of the REC in terms of averaged quantities such as the radar reflectivity, CG *flash* rate over a 20-min period centered on the time of the radar scan, and rain volume (calculated from reflectivity at the 2-km level using the convective Z–R relationship reported in Thiele et al. 1994).

Several characteristics of the lightning-producing convection observed during COARE are illustrated by the composite REC (Fig. 5). First, note that 30-dBZ reflectivities extended above the height of the −10°C level (~6.5 km) for approximately 20 min, coincident with an increasing CG flash rate and increasing cloud-top height (the latter defined by the 1-dBZ contour). Interestingly, a sharp increase in the number of CGs took place as the 30-dBZ contour reached its peak elevation. Furthermore, as the 20-, 30-, and 40-dBZ reflectivities began their descent, the cloud-to-ground lightning rate peaked and then fell off as the REC began to dissipate. The volume of rainfall produced by the REC exhibited only minor variations relative to the cloud-to-ground lightning evolution, with only a slight peak in rainfall occurring coincident with the peak in CG frequency. These observations further demonstrate the close coupling between the vertical distribution of hydrometeor mass in the mixed phase region of a cloud and the CG flash rate.

c. Satellite brightness temperature and cloud-to-ground lightning observations on 9 February 1993

Another useful way to examine CG lightning location data is to compare the CG return stroke positions

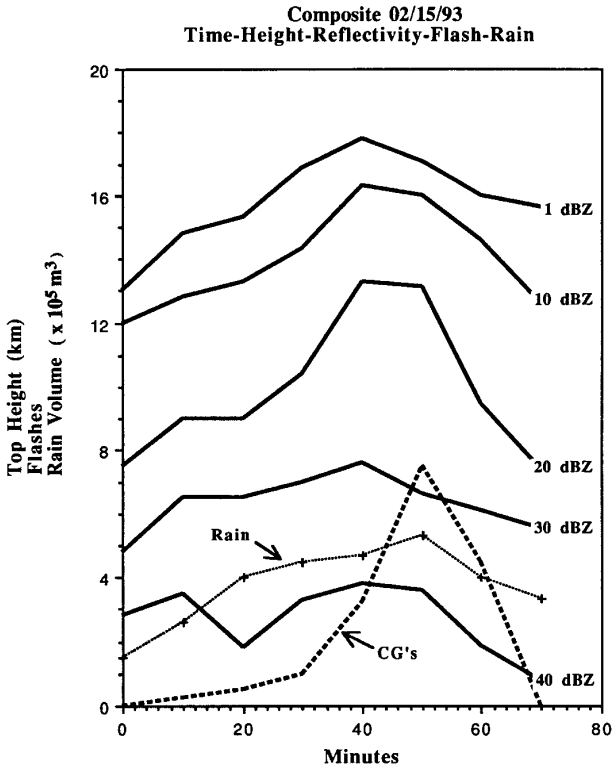

FIG. 5. Time–height, reflectivity, rain, and lightning frequency for 15 February 1993. Values of reflectivity echo-top height (km), CG flash number, and rain volume ($\times 10^5$ m^3) are indicated on the ordinate. The solid line represents the height of the labeled reflectivity threshold, the dashed line is the number of CGs for a 20-min period centered on the time of the radar scan, and the dotted line with crosses indicates the rain volume.

with IR satellite imagery (e.g., Goodman and MacGorman 1986). By overlaying the CG lightning positions on IR satellite data, one can make inferences regarding the location and to some extent the organization of intense convective cells (and presumably rainfall) situated beneath areally extensive cloud shields. GMS IR images for 9 February 1993 at 1045 and 1645 UTC, respectively, are shown in Figs. 6 and 8. The IR satellite images display cloud-top brightness temperatures (TBB) that were observed over the COARE domain. The positions of cloud-to-ground lightning *return strokes* (calculated using TOA techniques) that occurred within a 30-min period centered on the time of each respective satellite image are also indicated.

There are several interesting features associated with the first image (Fig. 6; 1045 UTC). First, the majority of the CG return strokes were associated with three clusters of clouds and areas of cold TBBs located to the south of the IFA near Bougainville Island (6°S, 155°E) and the northern tip of the Solomon Islands (7°S, 157°E). These CGs were likely associated with deep, vertically developed convection that formed over the islands, and subsequently propagated eastward over the warm pool. It is interesting to note that previous analysis times indicated that the CG lightning was confined primarily to the extreme eastern edge of the clusters while the coldest cloud tops extended over 150 km toward the west. This could be an indication that the cold cloud tops were associated with stratiform anvil or debris cloud, sheared in a westerly direction away from the most active convection (and heaviest rainfall) that was situated to the east of the islands (consistent with the orientation of the tropospheric shear vector during this period).

When the entire domain of Fig. 6 is examined, it is evident (at least this for this case) that regions of cloud-top temperature minima are rather poorly correlated to regions of cloud-to-ground lightning. For example, the cluster situated at 4°S, 160°E was associated with several large areas of cloud-top temperatures less than −65°C, yet no strokes were detected with this feature. As another example, consider the band of clouds that extended some 300 km northeast of the radar (located at approximately 2°S, 156°E). There are portions of the band with cloud-top temperatures colder than −65°C, yet there were no strokes associated with the clouds in the band.

The relationship between cloud-top height, satellite TBB, and degree of electrification in tropical oceanic clouds is dubious because 1) expansive areas of cold TBBs observed in the Tropics are often associated with stratiform cloud shields, raining, or nonraining that occur *after* the most intense period of convection in a cloud cluster and in general produce considerably less lightning than their convective counterparts (e.g., Rutledge and Petersen 1994); and 2) tropical oceanic convection is often very deep (i.e., cloud tops higher than

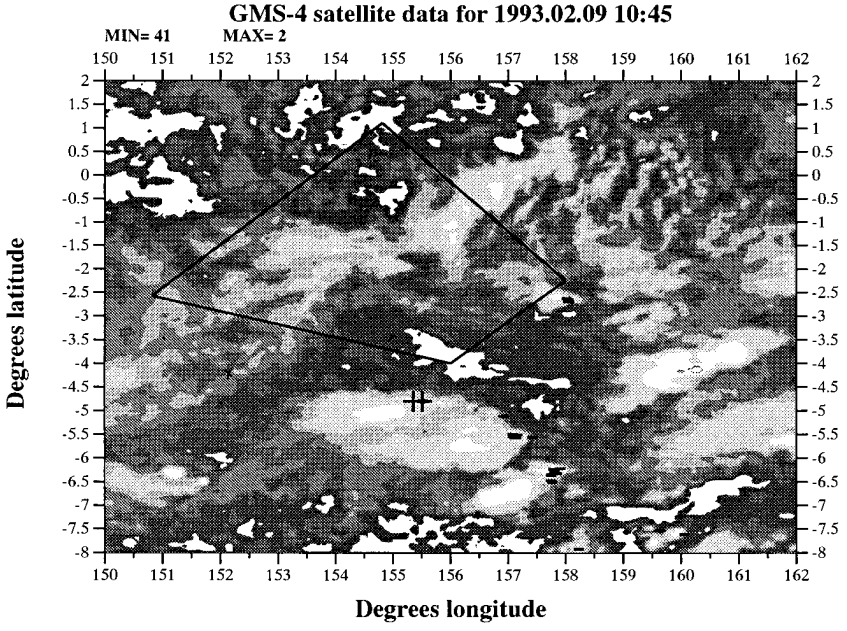

FIG. 6. GMS IR satellite imagery for 1045 UTC 9 February 1993. The shading intervals from dark to light indicate temperatures less than 15°, 0°, −15°, −30°, −45°, −65°, and −80°C. The COARE intensive flux array is indicated by the dark solid line. Positions of CG return strokes (hybrid TOA algorithm) for a 30-min period centered on the time of the satellite image. Return strokes of negative polarity are indicated with a dash, positive return strokes with a cross.

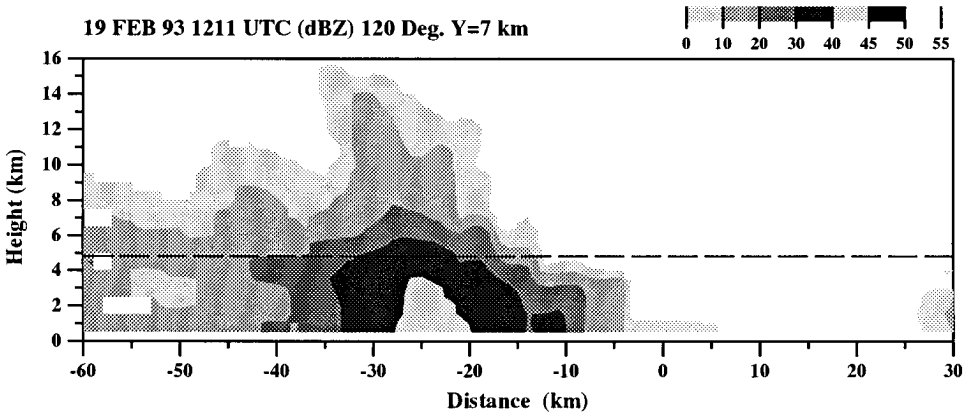

FIG. 7. Vertical cross section of MIT radar reflectivity for 19 February 1993 taken approximately normal to an approaching convective line. The radar was located at $X = 0$.

15 km) but only weakly electrified (i.e., producing little or no lightning). For example, a tall *but weakly electrified* cloud system observed on 19 February 1993 (1211 UTC) by the MIT radar is shown in a cross section of radar reflectivity in Fig. 7. These particular clouds were associated with very strong surface forcing concentrated along a gust front and possessed radar echo-tops of 15–17 km. Note, however, that the most significant hydrometeor mass in the cloud (as evidenced by reflectivities greater than 30 dBZ) was confined to elevations below the height of the freezing level, and thus, conditions were likely not favorable for significant electrification to occur. This type of observation is important to consider in parameterizations of lightning flash rates based on cloud-top height (e.g., Price and Rind 1994).

The last satellite observation to be discussed is presented in Fig. 8. At this time, the majority of the cloud-to-ground lightning was associated with a single large system situated near 4°S, 159°E. Note the rather linear organization of the strokes beneath the very cold cloud tops (i.e., <-80°C). Near this time, this same system was also being sampled by two NOAA P-3 aircraft in addition to the NCAR Electra, all three equipped with Doppler radars. The CG lightning pattern associated with the large area of cold cloud tops suggests that the most intense convection and heaviest rainfall at 1645 UTC was oriented in an approximately east–west line

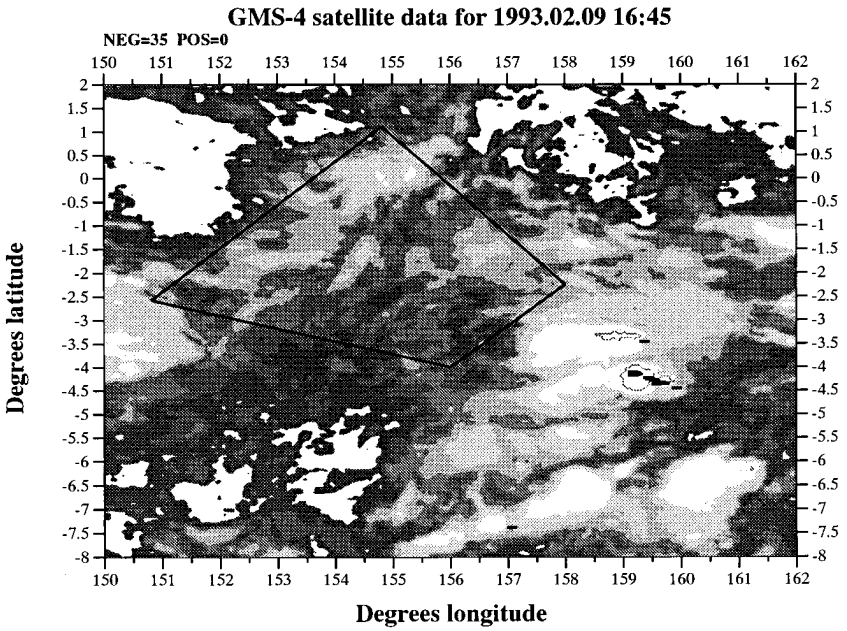

FIG. 8. As in Fig. 6 but for 1645 UTC.

with the western edge of the line being more intense. The general lack of cloud-to-ground lightning activity at 1645 UTC in the large area of cold cloud centered at approximately 3°S, 159°E is also consistent with the airborne radar observations. In this region airborne radar indicated that reflectivity values were considerably weaker and more stratiform in nature. The linear organization and spatial concentration of the lightning is consistent with the radar reflectivities and kinematic analyses previously reported for this case (Smull et al. 1994; Petersen et al. 1995).

Even though the majority of convection over the tropical oceans does not produce lightning (e.g., Figs. 6 and 8), the presence of lightning distinguishes deep, heavily raining oceanic convection from other cloud in an IR satellite image. This is an important point because recent rainfall amounts for the tropical western Pacific Ocean, estimated from both rain gauge and combined microwave and IR satellite retrievals, suggest that a disproportionate amount of the total rainfall (30%–40%) is produced by the deepest 1%–5% of tropical oceanic convection (e.g., Janowiak et al. 1994; Liu et al. 1995). Cloud-to-ground lightning location information collected by the COARE ALDF network may be able to provide important additional clues regarding the location, organization, and vertical structure of a small but important fraction of the deepest, heavily raining convection situated under extensive cold-cloud shields (as viewed from a satellite perspective) over the tropical western Pacific Ocean.

4. CAPE, wet-bulb potential temperature, and cloud-to-ground flashes

Rutledge et al. (1992) and Williams et al. (1992) found positive correlations between total lightning flash rates (in-cloud and cloud-to-ground) and 24-h average CAPEs for storms that occurred over the maritime continent of northern Australia (near Darwin). Their studies showed a marked increase in flash rate (peak values of nearly 60 flashes per minute) associated with monsoon-break periods when CAPE averaged approximately 1500–2000 J kg^{-1} and wet-bulb potential temperatures were 26°–29°C. Lower total flash rates (0–5 min^{-1}) were associated with modest values of CAPE (500–1000 J kg^{-1}) and low wet-bulb potential temperatures (~25°C) that occurred when a maritime airmass (monsoon trough) was situated over Darwin. Rutledge et al. used scaling arguments to explain the difference in flash rates between the two regimes (monsoon versus break), which ultimately related vertical velocities and mass at the particle balance level (BL; where the updraft speed equals the terminal fall speed of the precipitation particles) in the clouds to (CAPE)$^{1/2}$ and (CAPE)^3, respectively. Hence small increases in CAPE and updraft speed could significantly increase the amount of hydrometeor mass present at the BL in the mixed-phase region of the cloud, thereby increasing the electrical intensity and flash rate through noninductive charging processes (e.g., Williams and Lhermitte 1983). Williams et al. (1992) found a similar sensitivity between lightning frequency and surface wet-bulb potential temperature, which in turn was highly correlated to the CAPE (see also Williams and Renno 1993).

Because comprehensive sounding data were collected during TOGA COARE (Johnson et al. 1993), we were able to investigate the correlation between CAPE and the occurrence of cloud-to-ground lightning *flashes* (here we use flashes instead of return strokes) over the COARE domain. Given the results of Rutledge et al., a reasonable hypothesis would be that the electrical intensity of the warm pool convection *as inferred by the number of CGs produced in a given time period* should be correlated to the CAPE. To investigate this hypothesis, we used sounding data collected aboard the R/V *Vickers* during the time period 30 January 1993 to 26 February 1993 to calculate CAPE at 6-h intervals. We have confined our CAPE calculations for this section to those data collected aboard the R/V *Vickers* because the boundary layer moisture measurements were of high quality (J. Meywerk 1994, personal communication). Soundings launched in or near rain were not included in the sample. The temporal trend in the CAPE computed from the R/V *Vickers* sounding data is assumed to be representative of the domain of a 600 km × 600 km box centered on the *Vickers* that was also used to obtain CG flash totals. This assumption is supported by additional calculations, which indicate that CAPE values at the PRC 3 and PRC 5 ships (located some 220 km east and 120 km west, respectively, of the R/V *Vickers;* Fig. 1) varied in a similar fashion over the same time period.

The CAPE was calculated by lifting a parcel with thermodynamic properties characteristic of the lowest 50 mb of the sounding, pseudoadiabatically (neglecting ice processes) from the level of free convection to the equilibrium level. For several soundings that had missing data at upper levels but still had the boundary layer data, we calculated values of CAPE from a regression equation (based on approximately 100 points) that we developed to correlate the mean mixed-layer (50 mb deep) mixing ratio w_m (g kg^{-1}) and CAPE:

$$\text{CAPE} = 747.7w_m - 1.1538 \times 10^4. \qquad (1)$$

Given the strong correlation between the two variables ($r^2 = 0.91$), it is reasonable to calculate the missing CAPE values in this fashion. The resulting calculations yielded an overall mean CAPE of approximately 1800 J kg^{-1} for the entire 27-day time period with a standard deviation of approximately 600 J kg^{-1}. During convectively active periods (associated with more lightning) the CAPE often exceeded 2500 J kg^{-1}. During one 6-day period of little or no convective activity in the vicinity of the *Vickers* (early February 1993), the mean CAPE was lower than average with a mean of

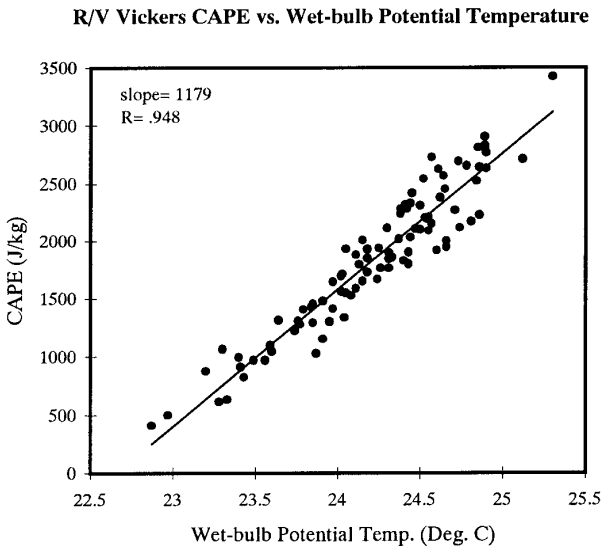

FIG. 9. Plot of CAPE (J kg^{-1}; ordinate) vs mixed-layer wet-bulb potential temperature (°C; abscissa) from the R/V *Vickers'* sounding data, 30 January–26 February 1993. The least squares regression line is also shown, with the slope and correlation coefficient indicated.

about 1000 J kg^{-1}. These results are comparable to previous estimates of CAPE made for other tropical oceanic environments (Zipser and LeMone 1980; Williams and Renno 1993).

From (1) we calculated a zero CAPE intercept corresponding to a mean mixed-layer mixing ratio (MLMR) of 15.4 g kg^{-1}. Interestingly, if one uses this value of MLMR and the mean mixed-layer potential temperature of approximately 301 K (calculated by compositing all nonraining soundings), a wet-bulb potential temperature θ_w (formulation in Bolton 1980) of approximately 22.6°C is obtained for a zero CAPE intercept. This θ_w value is very similar to the zero CAPE θ_w intercepts obtained by Williams and Renno (1993) for soundings taken over many other tropical locales. Indeed, when the correlation coefficient between the MLMR and θ_w was calculated, a strong positive correlation was found to exist ($R = 0.98$), suggesting that moisture variation in the boundary layer had a large effect on the value of θ_w. From Fig. 9, which is a plot of CAPE versus the mixed layer θ_w for the *Vickers'* soundings, it is clear that a strong relationship exists between θ_w and CAPE ($R = 0.95$). Furthermore, the value of the change, or sensitivity of CAPE with respect to θ_w (slope, 1179 J kg^{-1} C^{-1}) is very similar to the slope of 1150 J kg^{-1} C^{-1} reported by Williams and Renno (1993) for Ponape Island (7°N, 158°E), also located in the tropical western Pacific Ocean.

To examine the relative trends in CAPE and CG lightning over the 27-day period sampled, a time series of smoothed 24-h average CAPEs and smoothed 24-h CG flash totals (flashes that occurred in a 600 km × 600 km square centered on the R/V *Vickers*), was created (Fig. 10). The data presented in Fig. 10 indicate that a weak correlation (or common trend) does exist between the CAPE and the 24-h CG flash total over synoptic-scale time frames (i.e., time periods of several days). That is, cyclic increases or decreases in CAPE over the warm pool near the equator may to some extent modulate the frequency of occurrence and the intensity of electrified convection over the warm pool. Further, if the results of Fig. 10 are considered relative to the compouted relationship between θ_w and CAPE shown in Fig. 9, it appears that only a small change in the mean mixed-layer θ_w (recall the slope of 1179 J kg^{-1} C^{-1} θ_w) would be needed to produce a marked effect on the electrical intensity of convection over the western Pacific warm pool.

Indeed, the sensitivity of electrical intensity to θ_w is verified in Fig. 11, which compares smoothed θ_w's to smoothed numbers of CG flashes that occurred in the R/V *Vickers'* domain. The approximate mean θ_w (~24.25°C) for the points plotted in Fig. 11 is indicated by the bold arrow, along with the ''best-fit'' exponential curve. If we choose 1800 J kg^{-1} as the approximate mean CAPE in Fig. 10 and 2300 J kg^{-1} as an ''active'' CAPE (active electrically), we find from Fig. 9 that this is equivalent to approximately a 0.5°C increase in θ_w. In Fig. 11, a 0.5°C increase from the ''mean'' to ''active'' storm environment corresponds to a factor of 5 increase in CG lightning activity. Of course, a note of caution is warranted because this sample only represents approximately 30 days of data; however, the results are similar to those found in Williams (1992, 1994).

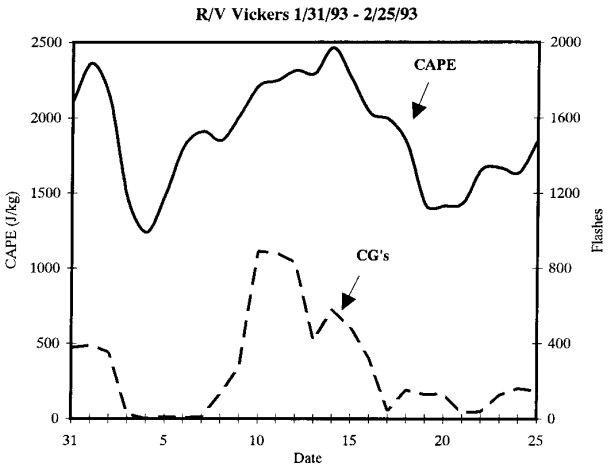

FIG. 10. The 31 January 1993 to 26 February 1993 plot of 24-h-averaged CAPE at the R/V *Vickers* (J kg^{-1}; solid line) and 24-h CG flash number (dotted line) in a 600 km × 600 km square centered on the R/V *Vickers*. A three-point smoother was applied to both the CAPE and lightning time series.

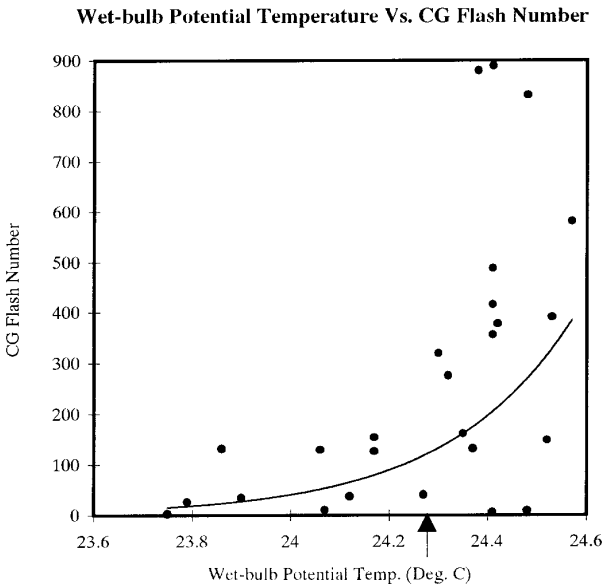

FIG. 11. The number of CG flashes in a 24-h period plotted against the 24-h mean mixed-layer wet-bulb potential temperatures (°C). Both fields were smoothed with a three-point filter. The mean wet-bulb potential temperature for the sample is indicated by a bold arrow. The ''best-fit'' exponential trend line for CG flash number as a function of wet-bulb potential temperature is indicated as a solid line through the points.

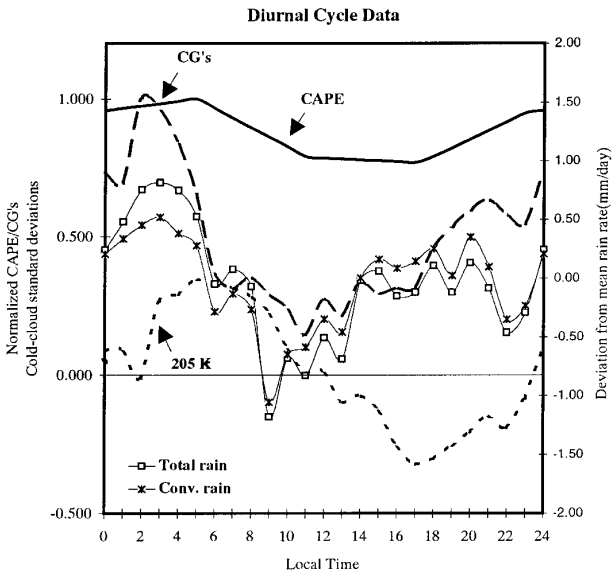

FIG. 12. The diurnal cycle of normalized CAPE (solid line), cloud-to-ground lightning (dashed line), cold-cloud area with brightness temperatures less than 205 K over a 30-day period (dotted line; plotted as a *Z* score), and total and convective rainfall [plotted as a deviation from the mean (mm day^{-1}) over a 90-day period], over the ocean ending 27 February 1993. Local time is indicated on the abscissa. The left ordinate indicates a normalized value for both CAPE and CG lightning and a *Z* score for the cold-cloud area coverage. The right ordinate indicates the deviation of rainfall from the mean in units of millimeters per day.

5. The diurnal cycle of CAPE, CG lightning, rainfall, and cold-cloud area

One additional test of the relationship between CAPE, flash rate, and the presence of deep, vertically developed convection is to examine the average diurnal cycle of all three variables. To examine the diurnal cycle of CAPE (Fig. 12), we composited CAPE's calculated at 6-h intervals (0000, 0600, 1200, and 1800 UTC) over approximately 30 separate days in the time period (22 January–26 February 1993) for the R/V *Vickers* and three other research vessels in the IFA (the R/V's *Moana Wave,* PRC 5, and PRC 3; Fig. 1). The magnitude of the CAPEs in Fig. 12 were then normalized to the peak CAPE of the composite to eliminate biases associated with systematic errors in the different ship sounding profiles; *here we wish only to examine the trend in the CAPE.* To determine the diurnal cycle of cloud-to-ground lightning *flashes* over the ocean, we constructed an ''ocean sector'' (Fig. 13) possessing an area of approximately 792 000 km^2. We then examined the frequency of all CG flashes that occurred in the ocean sector over 24, 1-h time bins, which provided a much larger sample spatially. Flashes were counted from a sample of 28 separate days in January and February 1993 (approximately 25 800 flashes).

To examine the diurnal cycle of deep tropical oceanic convection, we used areas of low satellite IR brightness temperature (cold-cloud areas) as a proxy for the occurrence of deep convective clouds. Cold-cloud areas were computed over the ocean sector (Fig. 13) for several different temperature thresholds. First, areas of cloudiness associated with brightness temperatures colder than 263, 255, 245, 235, 225, 215, 208, 205, and 195 K were summed over each 1-h period for the time period 30 January–28 February 1993. The sums of the areas were then normalized by the total area of the ocean sector used, and the mean normalized

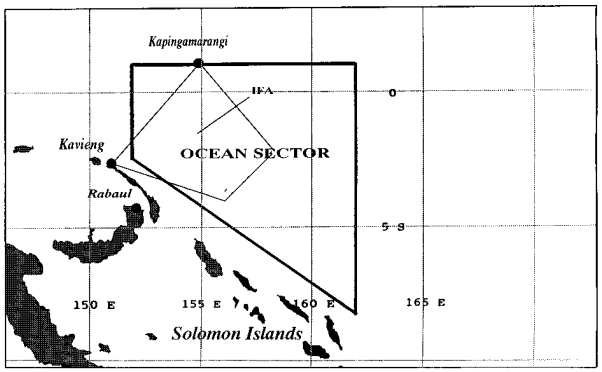

FIG. 13. A map of the approximate area covered by the ''ocean-sector'' (area within the bold-outlined polygon) used for calculating the diurnal cycle of CG lightning and cold-cloud area. The COARE IFA is contained within the smaller polygon (thin outline).

area in each temperature bin for the entire time period was calculated. Next, the mean normalized cold-cloud areas for each 1-h period of the day (same temperature thresholds as above) were calculated and subsequently plotted as a function of the number of standard deviations (*Z* score) from the mean normalized area calculated for the entire 30-day time period. The results indicated that weak diurnal cycles in cold cloudiness were present only for convection with brightness temperatures colder than 225 K (tops near 11.5 km). The diurnal signals were more pronounced for brightness temperatures less than 205 K (i.e., tops of at least 13.5 km). We have plotted the diurnal cycle of cloud-top brightness temperature less than 205 K in Fig. 12 for each 1-h bin as the number of standard deviations from the mean normalized area. To further emphasize the relationship between the diurnal cycle of CG lightning, cold-cloud area, and CAPE relative to that of precipitation, we have also added the diurnal cycle of convective and total rainfall to Fig. 12 (deviation from the mean over a 90-day time period; T. Rickenbach 1995, personal communication) for the approximate coverage area (70 000 km^2) of the MIT radar (situated aboard the R/V *Vickers;* Fig. 1). Note that the coverage area of the radar-rainfall estimate is smaller than the ocean sector area by a factor of 10, but the temporal sample of rainfall (90 days) is larger than that of the CAPE and CG lightning samples by a factor of 3.

In Fig. 12, the CAPE exhibits a broad, nocturnal-to-early morning maximum and a relative minimum at 1200 L. Both the CG lightning and rainfall appear highly correlated, exhibiting sharp peaks between 0200 and 0400 LT and broad minima similar to that of the CAPE centered near 1200 LT. The diurnal cycle of CG lightning also strongly resembles that of Lucas and Orville (1994), who analyzed a much larger sample of flash azimuths detected only at the Kavieng ALDF site. The peak in the diurnal cycle of CG lightning appears to precede the absolute peak in the diurnal cycle of the CAPE by approximately 3 h. Note, however, that the difference between the CAPE at 2300 and 0500 LT is very small (on the order of 100 J kg^{-1}) and that the soundings taken aboard the ships were collected at 6-h intervals. It is therefore possible that the actual peak in CAPE occurred between 2300 and 0500 LT.

The diurnal cycle of cold cloud temperatures below 205 K shown in Fig. 12 exhibits a weak (*Z* score only 0.3) but broad relative maximum in areal coverage near 0500 LT, approximately 2 h after the peak in the CG lightning and rainfall. The cold-cloud area begins a slow decline in coverage after 0900 LT, reaching a relative minimum in coverage near 1700 LT. It is interesting to note that as the CG lightning frequency and rainfall begin to increase near 1700 LT, the cold-cloud area reaches a minimum and begins to increase again, lagging the trend in CG lightning and rainfall by approximately 1–2 h. The increase in cold-cloud area coverage also seems to lag the increase in CAPE by several hours over the 24-h period. The weak diurnal cycle observed in the cold-cloud area is somewhat consistent with previous studies on the diurnal cycle of precipitation and cold-cloud area coverage over the western Pacific ocean (e.g., Gray and Jacobsen 1977; Nitta and Sekine 1994), though it must be emphasized that we have examined only a 30-d period.

The diurnal cycles of CAPE, flash rate, cold-cloud area, and rainfall suggest that increases in CAPE are associated with both increases in CG lightning and associated deep convection (consistent with the increase in cold-cloud area coverage and both the convective and total rainfall). The slight difference in phase between the peaks in CG lightning, total and convective rainfall, and the areas of cold cloudiness (cold-cloud area lagging lightning frequency and rainfall by 2 h), coupled with the observation that the cold cloudiness rapidly increases as the CG lightning and rainfall begin to peak (Fig. 12), suggests that the most intensely electrified convection and the heaviest rainfall occur before the maximum coverage of the cold-cloud area.

6. Summary

Herein we described the use of cloud-to-ground lightning location information gathered from the COARE ALDF network (Fig. 1). We concentrated primarily on lightning produced by clouds that occurred over the western Pacific Ocean in the vicinity of the COARE IFA. TOA and hybrid TOA methods yielded CG positions with estimated accuracies of approximately 10 km or less over distances approaching 900 km from the network. Positions calculated with TOA methods were then used for convective scale analyses (e.g., examining specific convective features). Cloud-to-ground lightning positions calculated by simple triangulation were included in larger-scale analyses (e.g., cycles of CAPE and lightning, diurnal cycle studies).

Examples of radar and satellite observations of oceanic convection together with CG lightning data were presented. Radar observations indicated that lightning-producing oceanic convection had reflectivities in excess of 30 dB*Z* in the mixed-phase region of the clouds and, consistent with many previous observations, CG flash rates that increased coincident with the descent of the reflectivity core aloft. Satellite and CG observations (Figs. 6 and 8) demonstrated the utility of the COARE ALDF network in pinpointing smaller areas of intense convection and rainfall embedded in areally expansive cold-cloud shields. For the cases shown, satellite estimated cloud-top heights (based on brightness temperatures) were a poor indicator for the presence of cloud-to-ground lightning. This is likely a reflection of the fact that clouds over the tropical western Pacific are often very deep, but lack the required hydrometeor mass in the mixed-phase region of the clouds to enable significant electrification to occur (e.g., Fig. 7), that is, they are not vertically developed.

To examine the relationship between CG lightning and larger-scale atmospheric variables such as CAPE, a 27-day time series of CAPE and cloud-to-ground lightning frequency was studied (Fig. 10). A weak positive correlation was found to exist between the CAPE and CG lightning in the 27-day time series, consistent with previous results from Rutledge et al. (1992) and others. When CAPE was compared to the mixed layer θ_w (Fig. 9), the results were very similar to those of Williams and Renno (1993) with regard to both the high correlation and sensitivity of CAPE to θ_w. Further, the frequency of CG lightning appeared to be very sensitive to small changes in the mixed layer θ_w ($\sim$0.5°C; Fig. 11) and modest changes in the CAPE ($\sim$500 J kg^{-1}).

Over a diurnal cycle, CAPE, CG lightning, and rainfall exhibited peaks and troughs that were approximately in phase, with the rainfall and CG lightning being the most highly correlated (Fig. 12). The cold-cloud area coverage exhibited a weak diurnal cycle with maxima and minima that lagged those of CG lightning frequency and the rainfall by approximately 2 h. Further, the rapid increase in cold-cloud area coverage that occurred nearly coincident with the peak in CG lightning and convective rainfall led us to hypothesize that the peak in cold-cloud area coverage may have been associated with large, cold, cirrus anvils that were preceded by intense convection (some associated with lightning) and heavy rainfall.

It is clear from these observations that a rather special set of circumstances must exist in a tropical oceanic convective cell and its environment before significant charge generation and lighting will occur. The fact that we now possess a cloud-to-ground lightning dataset that provides unprecedented information on the occurrence of CG lightning over the western Pacific Ocean will allow further identification of the dynamical and microphysical processes important to the electrification of oceanic convection over many different scales. Additionally, the noted sensitivity between lightning, which is associated with the cloud scale, and variables such as CAPE or θ_w that are affected by forcing on larger scales, suggests that lightning frequency measured on a global scale (e.g., from platforms such as the TRMM satellite; Simpson et al. 1988), could be used to detect small changes in climate variables such as θ_w over the tropical oceans [consistent with the findings of Williams (1992, 1994) and Price and Rind (1994)].

Acknowledgments: This research was supported under National Oceanic and Atmospheric Administration (NOAA) Grant NA37RJ0202 to Colorado State University (CSU), a National Aeronautics and Space Administration (NASA) Graduate Fellowship in Global Change Research NGT-30268 (W. Petersen), a NASA grant to CSU NAG 5-2692, and a National Science Foundation Grant ATM-9214835 to Texas A&M. We thank Steve Barnaby and Xing Li at Texas A&M for their efforts in processing the lightning data. We would also like to acknowledge all members of the MIT–CSU radar crew, the NOAA–TOGA radar crew, and the COARE lightning investigation team. The crew of the R/V *John V. Vickers* is also thanked for their outstanding service during COARE. The field mill on the R/V *Vickers* was supplied by E. Williams of MIT. D. Boccippio of MIT assisted with the operation and maintenance of the field mill. Mr. Tom Rickenbach, CSU, is acknowledged for contributing his work on the COARE diurnal cycle of rainfall to Fig. 12.

APPENDIX

Lightning Location Methods and Site Error Determination

Two return stroke location methods, magnetic direction-finding and time-of-arrival, were used by researchers at both Colorado State University (CSU) and Texas A&M University (A&M) to compute the locations of return stroke positions associated with cloud-to-ground lightning flashes (positions were calculated for each return stroke in a flash). Because the majority of research and data collected during COARE concentrated on atmospheric and oceanic processes that occurred over and near the IFA, initial efforts were concentrated on calculating stroke locations for areas in the vicinity of the IFA. For example, at CSU stroke locations were computed for the area located to the east of a line connecting Kapingamarangi, Kavieng, Rabaul, and a vector oriented along the 125° radial from Rabaul (Fig. 1).

a. Flash positions computed using triangulation

Cloud-to-ground return stroke locations were initially calculated independently at A&M and CSU using magnetic direction-finding techniques (i.e., triangulation). At CSU the triangulated positions were calculated using the intersection of azimuth bearings from two ALDFs and the law of sines on a sphere to determine a return stroke latitude and longitude. Because there were three ALDF antennas, when all three detected the same return stroke, three separate triangulations were possible. This yielded a set of three different positions for a given stroke that were initially averaged to arrive at the final stroke location. The triangulation calculation was completed in a similar fashion at A&M with the exception that a flat earth was assumed in the equations (in contrast to spherical geometry used at CSU). When the calculated positions were compared between the two groups, reasonably good agreement was found between the two sets of flash locations (i.e., locations were generally within 1–5 km of each other).

When all of the positions were calculated for a given time interval they were overlaid on radar and satellite data to provide additional checks on the location accuracy. As an example, Fig. A1 shows a horizontal

cross section of radar reflectivity at a height of 2 km collected on 1 February 1993 (0542 UTC) by the MIT C-band Doppler radar aboard the R/V *Vickers* (located approximately 400 km from the center of the ALDF network). The locations of cloud-to-ground lightning return strokes that occurred within a 20-min period centered on the radar analysis time are also indicated. It is clear that many of the triangulated return stroke positions were incorrect because it is unlikely that the lightning discharges were associated with areas of very low reflectivities or areas where no radar echoes were detected. Yet, the more general area of occurrence for the flashes appears plausible given the magnitude of the radar reflectivities (i.e., 45–50 dBZ) observed for some of the cells located in the same general vicinity.

To further examine the relative accuracy of the triangulated CG positions, we overlaid triangulated CG return stroke locations and GMS imagery collected on 9 February 1993 (1245 UTC; Fig. A2). Again, note the *broad* agreement near 6°S, 158°E between satellite brightness temperatures (proxy for cloud-top height) and the CG return stroke pattern. However, the triangulated lightning locations appear suspicious because of the relatively large scatter of the stroke locations in both cloudy and clear areas of the satellite imagery. Clearly, a method for more accurately locating the return stroke positions including quantification of the site errors associated with each antenna location was needed.

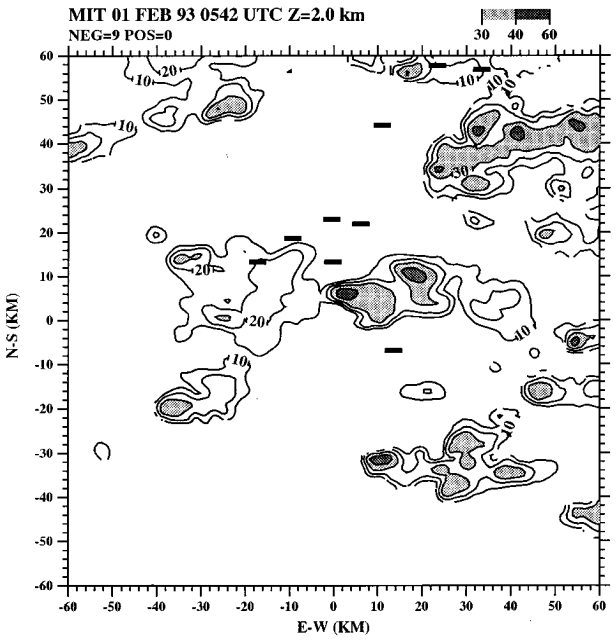

FIG. A1. As in Fig. 2 but with CG return stroke positions calculated using triangulation.

b. Development of TOA methods for locating cloud-to-ground flashes

To calculate more accurate CG stroke locations, it was necessary to develop a method that did not rely solely on the azimuth bearings to flashes because the bearings were contaminated by site errors. This was accomplished independently at CSU and A&M by developing algorithms for locating CG return strokes based on time-of-arrival methods (which do not require azimuth bearings). At A&M, the return stroke positions were computed using analytical solutions to the polynomial equations governing the intersection of two hyperbolas (hyperbolas determined by differences in the stroke detection time between two pairs of antennas). At CSU the same polynomial equations governing the intersections of two hyperbolas were developed, but the stroke locations (roots to the equations) were computed in a ''hybrid'' algorithm that used stroke locations previously calculated by triangulation as an *initial guess* in the TOA-type solution. We use the word ''hybrid'' because TOA techniques typically rely only on differences in arrival time between at least three (or more) antennas and the intersection of the resulting two (or more) hyperbolas to determine a flash location (e.g., Bent and Lyons 1984; Holle and Lopez 1993).

For the hybrid approach, the triangulated stroke locations were used to specify an initial interval (100-km radius from the triangulated position) for finding the root of the equation governing the intersection of two hyperbolas defined by the specific differences in time of arrival for a flash signal at different pairs of ALDFs. In this manner, the roots to the polynomial equations (i.e., the stroke locations) could be computed quickly and efficiently using the specified interval in a simple bisection algorithm. Because the initial guess for the return stroke position was assumed to be relatively close to the actual location of the stroke (i.e., within 100 km), the probability of calculating incorrect solutions because of the geometrical ambiguities involved (shown in Fig. A3) when using only three antennas for a TOA-type solution (Holle and Lopez 1993) should be reduced. Indeed, with the exception of strokes that occurred very close to ALDF sites, ambiguous location errors do not appear to be a problem.

Because the stroke positions were computed independently using slightly different algorithms (i.e., at CSU and at A&M), it was possible to compare the positions. The location comparisons revealed differences in CG stroke positions of only 1–3 km within a range of approximately 500 km from the center of the network. At longer ranges (i.e., 500–900 km from the network), the computed positions differed by as much as 7–10 km. Subsequent analysis revealed that the differences found to exist between the computed stroke locations in the two algorithms (especially at long ranges from the network) were due primarily to small differences in the constants and precision defined in the computer programs used to solve the intersection equa-

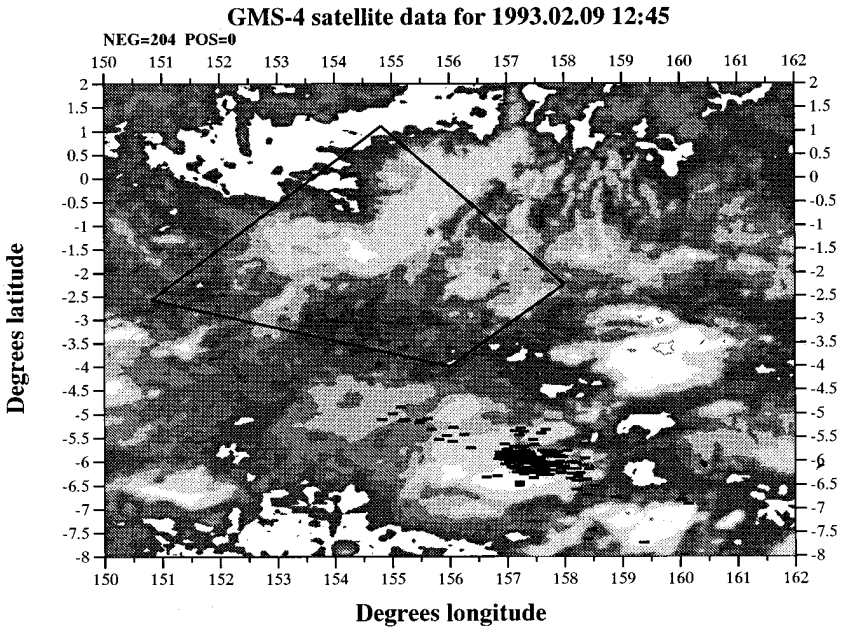

FIG. A2. As in Fig. 6 but for 1245 UTC. Lightning positions were calculated using triangulation.

tions (e.g., the radius of the earth, rotation angles, etc.). Given the relatively small differences in stroke location as a function of range between the two algorithms, it is clear that the two methods produced stroke locations that compare quite favorably for ranges approaching 900 km from the network.

An example of the marked increase in location accuracy due to implementation of the TOA algorithm can be inferred from Fig. 2 (case discussed in section 3.1), which is the same plot of radar reflectivities shown in Fig. A1, with the important exception that the overlaid CG stroke positions were computed using the hybrid TOA method. Note that the stroke positions are now clustered around more intense convective cells, located approximately 10 and 60 km northeast of the radar ($x = 10, y = 15$ and $x = 55, y = 45$, respectively). In particular, the cell and associated CGs closest to the radar were observed both from a visual and electronic perspective, the latter by an electric field mill operating on board the R/V *Vickers* (discussed in section 3.1).

We can gain further appreciation for the increased accuracy of the TOA techniques by examining the same satellite data shown in Fig. A2, but with the positions of CG flashes calculated by the hybrid TOA technique overlaid (Fig. A4). In Fig. A4 the CG flashes situated under the eastern edge of the deep cloud system at 6°S, 158°E are now tightly grouped into a mesoscale region (compare to Fig. A2). Note that the absolute number of CG flashes located with the TOA technique (157) is smaller than the 204 flashes located using triangulation. This is a reflection of the requirement for at least three antennas to detect a CG before that flash can be located using a TOA algorithm. (Approximately 50 of the CGs in Fig. A2 were detected by only two antennas.) Over a large sample of CG flashes (~25 800) we found that approximately 65% of the flashes detected by two of the COARE ALDF antennas were detected by all three antennas. Hence, when using TOA-located CG flashes, a bias toward lower numbers of CG flashes can occur in these data.

Based on the algorithm error checks and on subsequent plots of lightning, satellite, and radar information, we estimate the location accuracy of the TOA methods for the COARE ALDF network to be within 10 km of the true stroke location at ranges of 500–900

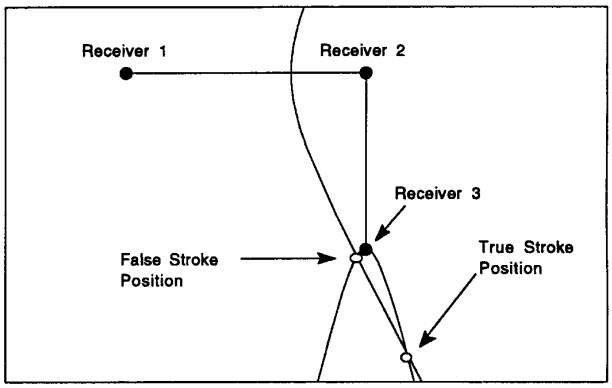

FIG. A3. Illustration of ambiguous location errors that can be encountered when only three DF antennas are used with the time-of-arrival solution. Note the two intersections of the hyperbola branches, and the true stroke position behind receiver 3 [reproduced from Holle and Lopez (1993)].

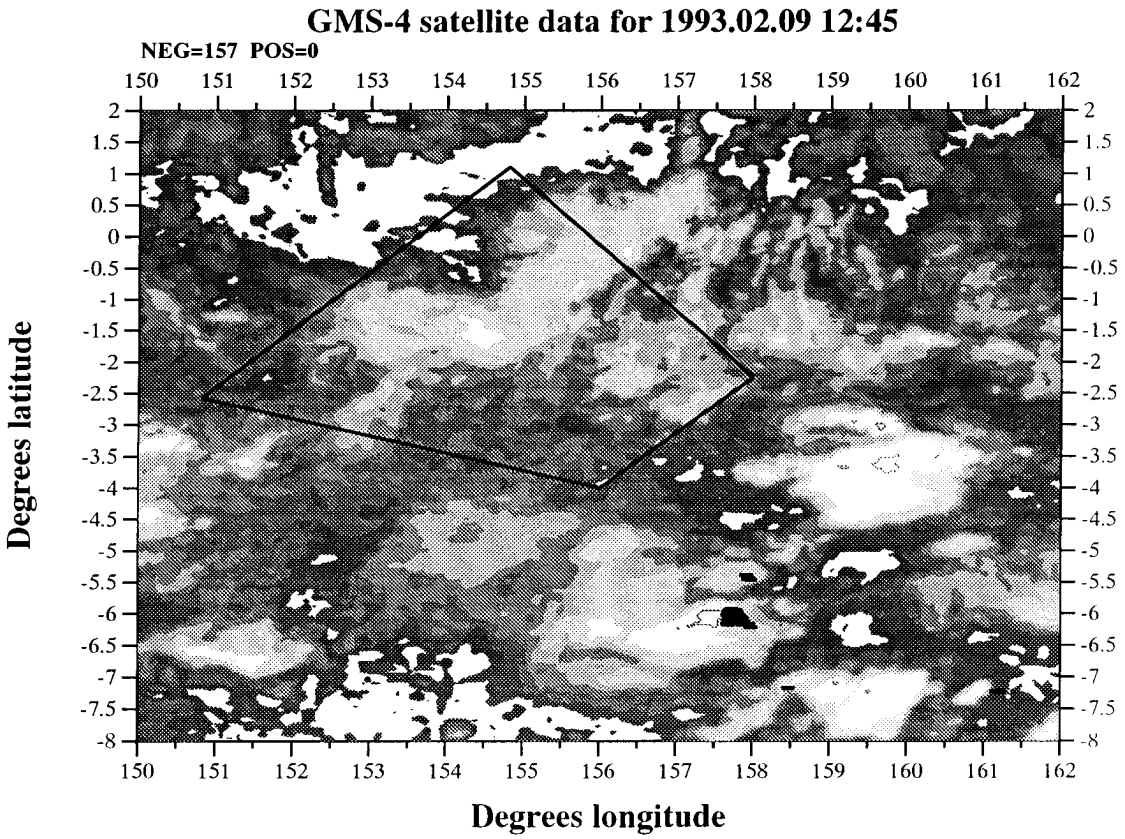

FIG. A4. As in Fig. A2 except the return stroke positions were calculated using the hybrid TOA algorithm. The CG return strokes are now located in two storm-scale groupings at 5.5°S, 158°E and 6°S, 158°E.

km from the network and within 2–5 km of the true location for ranges within 500 km of the network. These errors are remarkably low given the rather large distances at which cloud-to-ground lightning was detected by the network. Indeed, given the relatively small errors estimated for the location accuracy and the fact that no site error measurements could be performed for the network during or after installation, it seemed reasonable to use the TOA solutions for estimating site errors for each antenna.

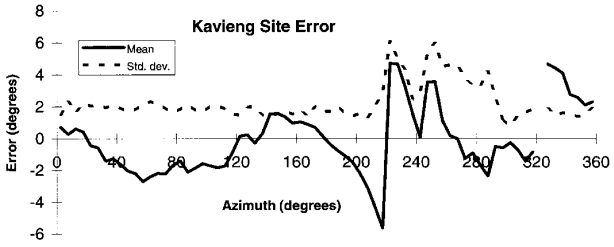

FIG. A5. An example of the site error curve (solid line) vs azimuth for Kavieng. The curve is based on data from the 26 most active lightning days from January through June 1993. The site error is evaluated for each 5° bin from 0° to 360°. The standard deviation (dashed curve) for each 5° azimuth bin is evaluated and plotted as a function of azimuth.

c. Estimation of antenna site errors

For a given CG return stroke detected by all three antennas, the algorithm for computing site errors (systematic errors in the measured azimuth to a flash for a given antenna) assumes that the stroke location determined by the TOA method is the actual location of the stroke. Subsequently, the azimuth to the assumed ''true'' location of the stroke can be computed for each antenna and then compared to the measured azimuths. The *mean* site error (with outliers removed) was then computed for 72 5° intervals (72 bins) by averaging the number of azimuth errors per bin for 26 separate days over a 6-month time period from January to June 1993. Subsequently, a site error curve (i.e., site error as a function of azimuth) and associated statistics such as the standard deviation of the site error for each azimuth bin could be created for each antenna (e.g., Kavieng ALDF; Fig. A5).

After examining the standard deviations of the site errors for many different azimuth bins (e.g., Fig. A5) and then plotting the frequency distributions of the site

errors for different azimuths, we found that 1) the error distributions were associated with standard deviations of approximately 2° in the majority of the bins; and 2) in some bins the number of individual azimuth errors was not a large enough sample (i.e., <30) to obtain accurate estimates of the mean and standard deviation of the site error for the bin. Visual inspection of the distributions (where a considerably higher number of strokes occurred) indicated that at least 30–50 strokes were required to obtain an accurate estimate of the mean site error for a bin. Standard deviations of 2° in the site error distribution for a particular azimuth seem reasonable (e.g., Tyahla and Lopez 1994) given that random errors in the measured azimuth for a single ALDF antenna are approximately 1°, and an additional error is introduced by our assumption that the TOA positions are the ''true'' locations of the strokes (i.e., in reality there is also an error associated with the locations calculated using the TOA method, though we have no way of directly assessing the value of that error).

Once site error curves were created, the errors were applied to the ALDF azimuths in an attempt to correct the antenna azimuths used in the triangulation algorithms. The triangulated positions were then recalculated and compared to the TOA solutions again. We found that for ranges less than 300 km from the center of the network, the corrected triangulations were within approximately 10–15 km of the TOA solutions, on average. However, the average errors found to exist between the corrected triangulations and the TOA solutions were typically much larger than 10 km at ranges greater than 300 km from the network. This would be expected even if all of the site error standard deviations were within 2° of the mean (i.e., a 2° error in azimuth places an azimuth bearing approximately 10 km from the true location of the stroke at a range of 300 km). Thus for ranges *exceeding* 300 km from the center of the TOGA COARE ALDF network, the accuracy of CG stroke positions calculated using *only triangulation* limits the application of the data to studies on larger scales that do not require accuracies of better than 10 km.

REFERENCES

Bent, R. B., and W. A. Lyons, 1984: Theoretical evaluations and initial operational experiences of LPATS (Lightning Position and Tracking System) to monitor lightning ground strikes using a time-of-arrival (TOA) technique. Preprints, *Seventh Int. Conf. on Atmospheric Electricity,* Albany, NY, Amer. Meteor. Soc., 1317–1324.

Blakeslee, R. J., and H. J. Christian, 1994: Lightning instrument package (LIP) for the ER-2 and DC-8 during TOGA COARE. *Proc. NASA Science Data Workshop-II,* Albuquerque, NM, NASA, 131 pp.

Bolton, D., 1980: The computation of equivalent potential temperature. *Mon. Wea. Rev.,* **108,** 1046–1053.

Brook, M., R. W. Henderson, and R. B. Pyle, 1989: Positive lightning strokes to ground. *J. Geophys. Res.,* **94,** 13 295–13 303.

Carey, L. D., and S. A. Rutledge, 1996: A multiparameter radar case study of the microphysical and kinematic evolution of a lightning producing storm. *J. Meteor. Atmos. Phys.,* **59,** 33–64.

Chauzy, S., M. Chong, A. Delannoy, and S. Despiau, 1985: The June 22 tropical squall line observed during COPT 81 experiment: Electrical signature associated with dynamical structure and precipitation. *J. Geophys. Res.,* **90,** 6091–6098.

Goodman, S. J., and D. R. MacGorman, 1986: Cloud-to-ground lightning activity in mesoscale convective complexes. *Mon. Wea. Rev.,* **114,** 2320–2328.

Gray, W. M., and R. W. Jacobson Jr., 1977: Diurnal variation of deep cumulus convection. *Mon. Wea. Rev.,* **105,** 1171–1188.

Hojo, J., M. Ishi, T. Kawamura, F. Suzuki, H. Komuro, and M. Shiogama, 1989: Seasonal variation of cloud-to-ground lightning flash characteristics in the coastal area of the Sea of Japan. *J. Geophys. Res.,* **94,** 13 207–13 212.

Holle, R. L., and R. E. Lopez, 1993: Overview of real-time lightning detection systems and their meteorological uses. NOAA Tech. Memo. ERL-NSSL-102, 73 pp.

Hughes, H. G., and R. J. Gallenberger, 1974: Propagation of extremely low-frequency (ELF) atmospherics over a mixed day-night path. *J. Atmos. Terr. Phys.,* **36,** 1643–1661.

Janowiak, J. E., P. A. Arkin, and M. Morrissey, 1994: An examination of the diurnal cycle in oceanic tropical rainfall using satellite and in-situ data. *Mon. Wea. Rev.,* **122,** 2296–2311.

Johnson, R. H., J. F. Bresch, P. E. Ciesielski, and W. A. Gallus Jr., 1993: The TOGA/COARE atmospheric sounding array: Its performance and preliminary scientific results. Preprints, *20th Conf. on Hurricanes and Tropical Meteorology,* San Antonio, TX, Amer. Meteor. Soc.

Jorgensen, D. P., T. Matejka, and J. D. DuGranrut, 1996: Multi-beam techniques for deriving wind fields from airborne Doppler radars. *J. Meteor. Atmos. Phys.,* **59,** 83–104.

Kitagawa, N., and K. Michimoto, 1994: Meteorological and electrical aspects of winter thunderclouds. *J. Geophys. Res.,* **99,** 10 713–10 721.

Krehbiel, P. R., 1986: The electrical structure of thunderstorms. *The Earth's Electrical Environment,* National Academy Press, 263 pp.

Krider, E. P., R. C. Noggle, and M. A. Uman, 1976: A gated, wide-band magnetic direction finder for lightning return strokes. *J. Appl. Meteor.,* **15,** 301–306.

Lhermitte, R. M., and E. R. Williams, 1984: Doppler radar and electrical activity observations of a mountain thunderstorm. Preprints, *22nd Conf. on Radar Meteorology,* Zurich, Switzerland, Amer. Meteor. Soc., 83–90.

Liu, G., J. A. Curry, and R. Sheu, 1995: Classification of clouds over the western equatorial Pacific Ocean using combined infrared and microwave satellite data. *J. Geophys. Res.,* **100,** 13 811–13 826.

Lucas, C., and R. E. Orville, 1994: TOGA COARE oceanic lightning. Preprints, *Symp. on Global Electrical Circuit, Global Change, and the Meteorological Applications of Lightning,* Nashville, TN, Amer. Meteor. Soc., 383–389.

Nitta, T., and S. Sekine, 1994: Diurnal variation of convective activity over the tropical western Pacific. *J. Meteor. Soc. Japan,* **72,** 627–641.

Orville, R. E., and D. W. Spencer, 1979: Global lightning flash frequency. *Mon. Wea. Rev.,* **107,** 934–943.

——, R. W. Henderson, and L. F. Bosart, 1983: An East Coast lightning detection network. *Bull. Amer. Meteor. Soc.,* **64,** 1029–1037.

——, and R. W. Henderson, 1986: Global distributions of midnight lightning: September 1977 to August 1978. *Mon. Wea. Rev.,* **114,** 2640–2653.

——, E. J. Zipser, and C. Weidman, 1994: TOGA COARE: Results from a lightning direction finder network in the remote western Pacific Ocean. Preprints, *Symp. on Global Electrical Circuit, Global Change, and the Meteorological Applications of Lightning,* Nashville, TN, Amer. Meteor. Soc., 378–382.

Petersen, W. A., and S. A. Rutledge, 1992: Some characteristics of cloud-to-ground lightning in tropical northern Australia. *J. Geophys. Res.*, **97,** 11 553–11 560.

——, ——, D. J. Boccippio, and E. R. Williams, 1993: The electrification of tropical oceanic convective clouds observed during TOGA-COARE. Preprints, *17th Conf. on Severe Local Storms/ Conference on Atmospheric Electricity*, St. Louis, MO, Amer. Meteor. Soc., 796–807.

——, R. Cifelli, S. A. Rutledge, and B. F. Smull, 1995: Cloud-to-ground lightning and the related kinematic structures of two tropical oceanic MCS's: Contrasting cases. Preprints, *Conf. on Cloud Physics*, Dallas, TX, Amer. Meteor. Soc., 553–564.

Price, C., and D. Rind, 1994: Possible implications of global climate change on global lightning distributions and frequencies. *J. Geophys. Res.*, **99,** 10 823–10 831.

Rutledge, S. A., and W. A. Petersen, 1994: Vertical radar reflectivity structure and cloud-to-ground lightning in the stratiform region of MCS's: Further evidence for in-situ charging in the stratiform region. *Mon. Wea. Rev.*, **122,** 1760–1776.

——, E. R. Williams, and T. D. Keenan, 1992: The Down Under Doppler and Electricity Experiment (DUNDEE): Overview and preliminary results. *Bull. Amer. Meteor. Soc.*, **73,** 3–15.

——, R. Cifelli, C. DeMott, W. Petersen, T. Rickenbach, J. Lutz, R. Bowie, M. Strong, and E. Williams, 1993: The shipboard deployment of the MIT C-band radar during TOGA COARE. Preprints, *26th Int. Conf. on Radar Meteorology*, Norman, OK, Amer. Meteor. Soc., 371–373.

Simpson, J., R. F. Adler, and G. R. North, 1988: A proposed Tropical Rainfall Measuring Mission (TRMM) satellite. *Bull. Amer. Meteor. Soc.*, **69,** 278–295.

Smull, B. F., D. P. Jorgensen, T. J. Matejka, and M. A. Lemone, 1994: Evolution of precipitation and momentum structure within a slow moving convective band observed by airborne Doppler radar during TOGA COARE. Preprints, *Sixth Conf. on Mesoscale Processes*, Portland, OR, Amer. Meteor. Soc., 21–24.

Takahashi, T., 1978: Electrical properties of oceanic tropical clouds at Ponape, Micronesia. *Mon. Wea. Rev.*, **106,** 1598–1612.

——, 1983: Electric structure of oceanic tropical clouds and charge separation processes. *J. Meteor. Soc. Japan*, **61,** 656–669.

——, and K. Kuhara, 1993: Precipitation mechanisms of cumulonimbus clouds at Pohnpei, Micronesia. *J. Meteor. Soc. Japan*, **71,** 21–31.

Thiele, O. W., D. A. Short, J. C. Gerlach, D. B. Wolff, M. J. McPhaden, and J. C. Wilkerson, 1994: TOGA COARE precipitation morphology. Preprints, *Sixth Conf. on Climate Variations*, Nashville, TN, Amer. Meteor. Soc., 91–95.

Turman, B. N., and B. C. Edgar, 1982: Global lightning distributions at dawn and dusk. *J. Geophys. Res.*, **87,** 1191–1206.

Tyahla, L. J., and R. E. L'opez, 1994: Effect of surface conductivity on the peak magnetic field radiated by first return strokes in cloud-to-ground lightning. *J. Geophys. Res.*, **99,** 10 517–10 525.

Uman, M. A., 1987: *The Lightning Discharge.* Academic Press, 377 pp.

University Corporation for Atmospheric Research, TOGA COARE International Project Office, 1993: TOGA COARE intensive observing period operations summary, 6.1.3.

Watson, A. I., and R. L. Holle, 1994: The relationship between cloud-to-ground lightning and WSR-88D VIL and cloud-top information. Preprints, *Symp. on Global Electrical Circuit, Global Change and the Meteorological Applications of Lightning*, Nashville, TN, Amer. Meteor. Soc., 325–331.

Webster, P. J., and R. Lukas, 1992: TOGA COARE: The Coupled Ocean–Atmosphere Response Experiment. *Bull. Amer. Meteor. Soc.*, **73,** 1377–1416.

Williams, E. R., 1992: Schumann resonance: A global tropical thermometer. *Science*, **256,** 1184–1187.

——, 1994: Global circuit response to seasonal variations in global surface air temperatures. *Mon. Wea. Rev.*, **122,** 1917–1929.

——, and R. M. Lhermitte, 1983: Radar tests of the precipitation hypothesis for thunderstorm electrification. *J. Geophys. Res.*, **88,** 10 984–10 992.

——, and N. Renno, 1993: An analysis of the conditional instability of the tropical atmosphere. *Mon. Wea. Rev.*, **121,** 21–36.

——, M. E. Weber, and R. E. Orville, 1989: The relationship between lightning type and convective state of thunderclouds. *J. Geophys. Res.*, **94,** 13 213–13 220.

——, S. A. Rutledge, S. C. Geotis, N. Renno, E. Rasmussen, and T. Rickenbach, 1992: A radar and electrical study of tropical hot towers. *J. Atmos. Sci.*, **49,** 1386–1395.

Workman, E. J., and S. E. Reynolds, 1949: Electrical activity as related to thunderstorm cell growth. *Bull. Amer. Meteor. Soc.*, **30,** 142–149.

Young, K. C., 1993: *Microphysical Processes in Clouds.* Oxford University Press, 427 pp.

Zipser, E. J., and M. A. LeMone, 1980: Cumulonimbus vertical velocity events in GATE. Part II: Synthesis and model core structure. *J. Atmos. Sci.*, **37,** 2458–2469.

——, and K. R. Lutz, 1994: The vertical profile of radar reflectivity of convective cells: A strong indicator of storm intensity and lightning probability. *Mon. Wea. Rev.*, **122,** 1751–1759.